

J. Environ. Treat. Tech. ISSN: 2309-1185

Journal web link: https://dormaj.org/index.php/jett https://doi.org/10.47277/JETT/9(4)780



# Enhanced Adsorption of Methylene Blue by Chemically Modified Materials Derived from *Phragmites australis* Stems

Bui Thi Minh Nguyet<sup>1\*</sup>, Nguyen Van Hung<sup>1\*</sup>, Nguyen Huu Nghi<sup>1</sup>, Nguyen Anh Tien<sup>2</sup>, Dinh Quang Khieu<sup>3</sup> and Hà Danh Đức<sup>1\*</sup>

<sup>1</sup>Dong Thap University, Cao Lãnh City, 81000, Vietnam <sup>2</sup>Ho Chi Minh City University of Education, Ho Chi Minh City, 748342, Vietnam <sup>3</sup>University of Sciences, Hue University, 530000, Vietnam

#### Abstract

Methylene blue (MB) is extensively used in various industries, resulting in severe environmental pollution. In this study, raw *Phragmites australis* biomass (RPB) chemically modified with sodium hydroxide (S-RPB) followed with citric acid (SA-RPB) for adsorbing MB from aqueous solutions was developed. The obtained adsorbents were characterized via X-ray diffraction (XRD), Brunauer–Emmett–Teller (BET), Fourier-transform infrared spectroscopy (FTIR), and pHpzc analysis. The batch adsorption tests showed that the MB removal efficiency of the SA-RPB absorbent was higher than that of RPB and S-RPB. The XRD results showed that the adsorbents existed mainly as cellulose crystals. The BET analysis indicated that the chemically modified materials formed micropores, with the capillary diameter of SA-RPB was 15.97 nm on average. The FTIR results confirmed a significant enhancement of hydroxyl and carboxyl groups on SA-RPB surface after denaturation by citric acid. The adsorption kinetics showed that the pseudosecond-order model precisely simulated the adsorption process. The adsorption isotherm process satisfactorily fitted with the Langmuir model, and the maximum adsorption capacity of SA-RPB was 191.49 mg/g at 303 K. The adsorption mechanism of MB onto the SA-RPB was mainly influenced by electrostatic interactions, hydrogen bonding, π–π stacking, and capillary filling of micropores. The adsorptive capacity exceeded 90% after four successive regeneration cycles and reuse of SA-RPB. These findings show that the adsorbent developed from raw biomass of *Phragmites australis* modified with NaOH and citric acid can be applied to remove MB from aqueous solutions.

Keywords: Methylene blue, Phragmites australis, Removal efficiency, Kinetics, Adsorption mechanism

# 1 Introduction

Dyes have been extensively used in industries, such as textile, leather, cosmetics, tanning, paper, food technology, hair coloring, pulp mill, pharmaceuticals, and plastics [1]. The wastewater discharged from these industries causes severe environmental pollution [2]. Among different dyes, methylene blue (MB) is the most widely used for coloring cotton, wood, and silk [3]. MB can damage the eyes of humans and animals. Moreover, MB triggers nausea, vomiting, profuse sweating, and mental instability when it passes through the mouth, and it causes rapid or difficult breathing within short periods after inhaling [4]. Therefore, it is necessary to remove MB from wastewater.

Many advanced techniques have been developed for removing MB. Examples include the Fenton process and combined electrochemical treatments [5], electrochemical degradation [6], reverse osmosis [7], photodecomposition [8], coagulation/flocculation [9], membrane processing [10], oxidative degradation [11], electrocoagulation [12], and carbonaceous nanomaterials [13]. Activated carbon is widely and effectively used for removing different dye molecules [14, 15]. However,

these methods are expensive, owing to poor regeneration. In recent years, considerable efforts have been made in developing natural and low-cost biosorbents, such as biopolymers [16], mango peels [17], modified *Ceiba pentandra* seeds [18], chestnut husk [19], peach stone [20], carbonized watermelon [21], and seed fibers [22], potato peels [23].

P. australis is a type of reed that mainly grows around lakes, rivers, streams, and brackish water worldwide between 10° and 70° northern latitude [24]. The plant has a high tissue porosity [25] formed by cellulose, hemicellulose, and lignin, which are vital constituents for developing absorbents. In previous studies, low-cost adsorbents were generated from P. australis biomass and used to remove MB [26, 27]. In these studies, MB adsorption was conducted using a raw material [27] and a raw material modified with NaOH [26]. Plant materials modified with citric acid show good potential for wastewater treatment [20, 28, 29]. In this study, cellulose fibrils extracted from P. australis were chemically modified with NaOH and citric acid and used to adsorb MB from liquid media. In addition, the effects of environmental parameters on the MB adsorption of raw and modified adsorbents were

nguyenvanhung@dthu.edu.vn. (c) Hà Danh Đức, Dong Thap University, Cao Lãnh City, 81000, Vietnam, E-mail: hadanhduc@gmail.com

<sup>\*</sup>Corresponding authors: (a) Bui Thi Minh Nguyet, Dong Thap University, Cao Lãnh City, 81000, Vietnam, E-mail: btmnguyet@dthu.edu.vn, and (b) Nguyen Van Hung Dong Thap University, Cao Lãnh City, 81000, Vietnam, E-mail:

evaluated. The integrated analysis of experimental and theoretical results provided important insights into the adsorption mechanism and efficient treatment of MB using the developed adsorbents.

# 2 Materials and Methods

#### 2.1 Chemicals and materials

Citric acid (HOC(COOH)(CH<sub>2</sub>COOH)<sub>2</sub>,  $\geq$  99.5%), sodium hypophosphite monohydrate (NaH<sub>2</sub>PO<sub>2</sub>.H<sub>2</sub>O,  $\geq$  99.5%), sodium hydroxide (NaOH,  $\geq$  97%), hydrochloric acid (HCl, 37%), sodium chloride (NaCl,  $\geq$  99.5%), and MB (C<sub>16</sub>H<sub>18</sub>N<sub>3</sub>SCl, 99.5%) were purchased from Sigma-Aldrich. The MB was diluted with double-distilled water to a range of 125–300 mg/L. The pH was adjusted using NaOH (0.1 M) and HCl (0.1 M).

Plant samples of *P. australis* gathered from a wetland in Dong Thap province, Vietnam were used for experiments. The plants were cleaned with tap water to remove dirt and other impurities adhered to their surfaces. The plant stems were collected and dried under the sun for four days before being finely ground to approximately 1–2 mm sizes. The obtained biomass was rinsed with distilled water and dried in a vacuum oven at 70 °C to a constant weight. The product was stored in a desiccator and used as raw *P. australis* biomass (RPB).

# 2.2 Chemical modifications of P. australis biomass

RPB (5 g) was added to a 250 mL glass beaker containing 100 mL NaOH (0.5 M). The solution was stirred at 60 °C and 400 rpm using a magnetic bar for 5 h. The biomass was collected and cleaned with distilled water until the pH of the solution was 7.0. The product was then dried in a vacuum oven at 60 °C for 12 h to yield an adsorbent. The biomass modified with NaOH was designated as S-RPB. The S-RPB material was further denatured using a citric acid solution. Fifty milliliters of citric acid solution (0.1 M) was added to a 2.0 g S-RPB. NaH<sub>2</sub>PO<sub>2</sub>.H<sub>2</sub>O (2.65 g), used as a catalyst, was added to the solution. The biomass was collected after stirring at 60 °C and 400 rpm using a magnetic bar for 5 h. The biomass was soaked in 50 mL distilled water several times until the pH became 7.0, and it was dried at 60 °C for 12 h, and subsequently, at 140 °C for 3 h. The second modified adsorbent was designated as SA-RPB.

#### 2.3 Characterization of materials

The lignocellulosic composition before and after modification was determined according to the National Renewable Energy Laboratory (NREL) compositional analysis procedure [30]. The C, H, N, S, and O contents of the materials were analyzed using a CHNS-O Elemental Analyzer (Thermo, Flash EA1112, USA). XRD of the products was performed using a MiniFlex 600 diffractometer (Rigaku, Japan) with a radiation source of Cu Kα, λ = 0.15406 nm. The scanned angle (20 values) ranged between  $5^{\circ}$ and 80° with a step size of 0.01°. The surface morphology of the adsorbents was scanned using the scanning electron microscopy (SEM) technique (FEI-SEM NOVA NanoSEM 450-USA). FTIR spectra of the samples were recorded using an Infrared Affinity-1S spectrophotometer (Shimadzu). BET was determined using N2 adsorption-desorption isotherms at liquid nitrogen temperature (77 K) using a Quantachrome TriStar 3000 V6.07A adsorption instrument.

# 2.4 Determination of point of zero charge (pH<sub>PZC</sub>)

The pH<sub>PZC</sub> of the adsorbents was determined using the pH drift method described in a previous study [31]. Forty-five milliliters of 0.5 M NaCl with pH values were adjusted from 2 to 12 using 0.1 M NaOH or 0.1 M HCl solutions. Distilled water (50 mL) was added, and the pH values were readjusted and considered the initial pH (pH<sub>i</sub>). Next, an adsorbent was added to each flask at 1.0 g/L,

incubated at 180 rpm using a magnetic stir bar for 24 h at room temperature ( $\sim$ 30 °C). The differences in the pH ( $\Delta$ pH) values between the initial pH and final pH (pH<sub>f</sub>) ( $\Delta$ pH = pH<sub>i</sub> – pH<sub>f</sub>) were plotted against pH<sub>i</sub>. The points of intersection of the curve with the abscissa at which  $\Delta$ pH is equal to zero were presented as the pH<sub>PZC</sub>.

#### 2.5 Adsorption tests

Adsorption tests were performed by adding an adsorbent to a 250 mL glass beaker containing 100 mL MB solution. For the effects of MB concentrations of adsorption, the MB was diluted to 125–300 mg/L. For the effects of the adsorbent on adsorption, SA-RPB (0.4–1.4 g/L) was used. The solution was stirred at 300 rpm, and liquid media were collected from 2 to 105 min. Liquid media samples were centrifuged at 3000 rpm for 5 min to remove solid particles. MB concentrations were measured using an ultraviolet–visual spectrophotometer (Spectro UV–2650, Labomed, USA) at a wavelength of 665 nm. The percent removal (R) and adsorption capacity per unit mass (R) after a specific contact time (R) were calculated using Eqs. (1) and (2), respectively:

$$R(\%) = \frac{C_o - C_t}{C_o} \times 100 \tag{3}$$

$$q_t = \frac{(C_o - C_t) \times V}{m} \tag{2}$$

where  $C_0$  (mg/L) and  $C_t$  (mg/L) are the MB concentrations in liquid media at the initial and time t, respectively, and V is the volume of the solution (L).

#### 2.5.1 Adsorption kinetics

The adsorption kinetics were fitted to the pseudo-first-order and pseudo-second-order kinetic models. The pseudo-first-order [32] and pseudo-second-order (Ho & McKay 1999) [33] equations are expressed by Eqs. (3) and (4), respectively:

$$q_t = q_e (1 - e^{-k_1 t}) (3)$$

$$q_t = \frac{q_e^2 k_2 t}{1 + q_e k_2 t} \tag{4}$$

where  $k_1$  (min<sup>-1</sup>) and  $k_2$  (g/mg.min) are the rate constants of the pseudo-first-order and pseudo-second-order, respectively, and t (min) is the contact time.

# 2.5.2 Adsorption isotherms

Four isotherm equations, that is, the Langmuir, Freundlich, Temkin, and Dubinin–Radushkevich equations, were used to fit the experimental equilibrium isotherm data for the MB adsorption on SA-RPB. Adsorption isotherm tests were performed by adding 0.1 g SA-RPB into 100 mL MB (150 mg/L). The initial pH of the MB solution was 6.5, and the controlled temperatures were 30 °C (303 K), 40 °C (313 K), and 50 °C (323 K). The Langmuir model assumes that adsorption is localized on a monolayer, and all adsorption sites on the adsorbent are homogeneous and possess the same adsorption capacity [34], as expressed by Eq. (5):

$$q_e = \frac{q_{max} K_L C_e}{1 + K_L C_e} \tag{5}$$

where  $C_e$  (mg/L) is the equilibrium concentration,  $q_e$  (mg/L) is the amount of adsorbed dye at equilibrium,  $q_{\text{max}}$  (mg/g) is the maximum adsorption capacity, and  $K_L$  (L/mg) is the Langmuir adsorption equilibrium constant. The equilibrium parameter ( $R_L$ ) is

a dimensionless constant of the Langmuir isotherm, expressed by Eq. (6) [35]:

$$R_L = \frac{1}{1 + K_L C_o} \tag{6}$$

where  $C_0$  is the highest initial solute concentration. The Freundlich isotherm model Freundlich [36] assumes multilayer adsorption processes occur on heterogeneous surfaces, expressed by Eq. (7):

$$q_e = K_F C_e^{1/n_F} \tag{7}$$

where  $K_F$  (mg/g.(L/mg)<sup>1/n</sup>) and n are Freundlich constants related to the adsorption capacity and adsorption intensity, respectively. The adsorbate—adsorbate interactions can cause a decrease in the heat of adsorption of all the molecules in the layer. The Temkin isotherm [37] reflects the effect of the adsorbate interaction on SA-RPB, expressed by Eq. (8):

$$q_e = \left(\frac{RT}{b}\right) \ln(A_T C_e) \tag{8}$$

$$B_T = \frac{RT}{h} \tag{9}$$

where  $A_t$  (L/g) and b (g.J/mg.mol) are Temkin's isotherm constants, R (8.314 J/mol.K) is the universal gas constant, and T (K) is the absolute temperature. The Dubinin–Radushkevich isotherm [38] can be applied to examine the characteristics, free energy, and porosity of any adsorbent. The model has been used to determine the mean free energy of biosorption, expressed by Eqs. (10)–(12):

$$q_e = q_{DR}e^{-K_{DR}\varepsilon^2} (10)$$

$$E = 1/\sqrt{2K_{DR}} \tag{11}$$

$$\varepsilon = RT \ln(1 + \frac{1}{C_0}) \tag{12}$$

where  $K_{DR}$  is a constant related to the adsorption energy (mol<sup>2</sup>/kJ<sup>2</sup>),  $q_{DR}$  (mg/g) is the Dubinin–Radushkevich isotherm adsorption capacity,  $\varepsilon$  (kJ/mol) is the Polanyi potential, R is the ideal gas constant, and T (K) is the temperature. The free energy of adsorption (E) is considered as chemical adsorption (E = 8–16 kJ/mol) or physical adsorption (E < 8 kJ/mol).

# 2.5.3 Adsorption thermodynamics

The thermodynamic parameters for the MB adsorption onto SA-RPB were evaluated at 303, 313, and 323 K. Gibb's free energy change ( $\Delta G^{\circ}$ ), enthalpy ( $\Delta H^{\circ}$ ), and entropy ( $\Delta S^{\circ}$ ) were calculated using Eqs. (13)–(15).

$$\Delta G^o = -RT ln K_L \tag{13}$$

$$\Delta G^o = \Delta H^o - T \Delta S^o \tag{14}$$

The combination of Eqs. (13) and (14) yields Eq. (15):

$$lnK_L = -\frac{\Delta H^o}{RT} + \frac{\Delta S^o}{R} \tag{15}$$

where R (8.314 J/mol.K) is the universal gas constant, T (K) is the absolute temperature, and  $K_L$  is the Langmuir equilibrium constant. The values of  $\Delta H^o$  and  $\Delta S^o$  can be calculated from the slope and intercept, respectively, of the linear plot of  $\ln K_L$  versus 1/T.

#### 2.5.4 Parameter estimation

Kinetic and equilibrium models were fitted to the adsorption models through linear and nonlinear regressions using Origin 2018 software (OriginLab, USA). The fit of goodness was determined using the correlation coefficient ( $R^2$ ) and chi-square ( $\chi^2$ ) equations:

$$R^{2} = 1 - \frac{\sum_{n=1}^{n} (q_{e,exp} - q_{e,cal})^{2}}{\sum_{n=1}^{n} (q_{e,exp} - \bar{q}_{e,exp})^{2}}$$
(16)

$$\chi^{2} = \sum_{n=1}^{n} \left( \frac{(q_{e,exp} - q_{e,cal})^{2}}{q_{e,cal}} \right)$$
 (17)

where  $q_{e,cal}$  and  $q_{e,exp}$  are the calculated and experimental data, respectively.

#### 2.6 Reusability

After each cycle of batch experiment, the SA-RPB was first washed with absolute ethanol and subsequently washed with double-distilled water three times. The adsorbent was then dried for 24 h at  $100\ ^{\circ}\text{C}$  until its weight became constant.

#### 3 Results and discussion

#### 3.1 Characterization of materials

The biomass components of *P. australis* are listed in Table 1. The components of the raw RPB were also determined in previous studies [39, 40]. The cellulose content significantly increased, whereas hemicellulose and lignin contents comparatively decreased after treatment with NaOH (S-RPB) and NaOH followed with citric acid (SA-RPB) (Table 1). The C concentration decreased slightly, whereas the O concentration and the ratio of O to C increased slightly. Moreover, the percentages of N, S, Si, K, and Mg significantly decreased after treatment. Acidic and basic solutions are typically used for modifying and/or removing lignin and hemicellulose from plant biomass [41]. The treatment with NaOH resulted in the formation of hydroxyl groups on the S-RPB, which then reacted with citric acid, forming an ester linkage to introduce carboxyl groups into the SA-RPB [20].

SEM micrograph images of P. australis biomass before and after treatment with NaOH and citric acid were captured (Figure 1). The raw material had a smooth, nonporous surface composed of fibrous rods (Figure 1(a)). The surface morphology changed after denaturing with NaOH. The S-RPB sample retained its tubular structure, but the surface became more porous and irregular (Figure 1(b)). The surface became rougher and more irregular after treatment with NaOH, followed by citric acid treatment (Figure 1(c)). The crystallographic structures of RPB, S-RPB, and SA-RPB were analyzed using the XRD technique (Figure 1(d)). The results indicated that all samples had two diffraction peaks at angles 20 of 15.7° and 22.3°, corresponding to (101) and (002) planes of cellulose crystals [42]. The diffraction intensities were in the order of SA-RPB > S-RPB > RPB (Figure 1(d)), indicating that NaOH and citric acid enhanced the cellulose crystallinity. Increased crystallization attributed to the partial removal of amorphous polymers (hemicellulose and lignin) from plant structures has also been reported [26, 43]. The specific surface area and porous texture of the obtained samples were evaluated using the nitrogen adsorption-desorption isotherms at 77 K (Table 2). The RRB sample had a specific surface area of 1.01 m<sup>2</sup>/g, a common property of raw plant biomasses [44]. The surface areas decreased by 13.9% after treatment with NaOH and 26.7% after treatment with NaOH and citric acid. The corresponding data for the volumes were 21.8% and 26.3%. However, the average pore diameter was somewhat stable after treatments. Citric acid can easily penetrate the pore structure because of its small molecular size [45].

Table 1: Chemical compositions of RPB, S-RPB, and SA-RPB

Parameter	RPB	S-RPB	SA-RPB
Lignocellulosic analysis (dry weight basis), wt%			
Cellulose (%)	43.31	66.32	71.21
Hemicellulose (%)	30.82	15.17	13.28
Lignin (%)	20.37	12.30	9.19
Elemental analysis (dry weight basis), wt%			
C (%)	46.42	45.71	45.23
O (%)	45.82	47.72	48.83
H (%)	5.910	5.610	5.720
N (%)	0.232	0.111	0.021
S (%)	0.313	0.222	0.107
O/C (mol/mol)	0.7403	0.7830	0.8097
Si (%)	1.050	0.021	-
K (%)	0.454	0.284	0.182
Mg (%)	0.601	0.322	0.110

Table 2: Porous textural parameters of RPB, S-RPB, and SA-RPB samples

Sample	Surface area (m <sup>2</sup> /g)	Pore volume (dm <sup>3</sup> /g)	Average pore diameter (nm)
RPB	1.01	2.626	16.64
S-RPB	0.87	2.052	16.86
SA-RPB	0.74	1.935	15.97

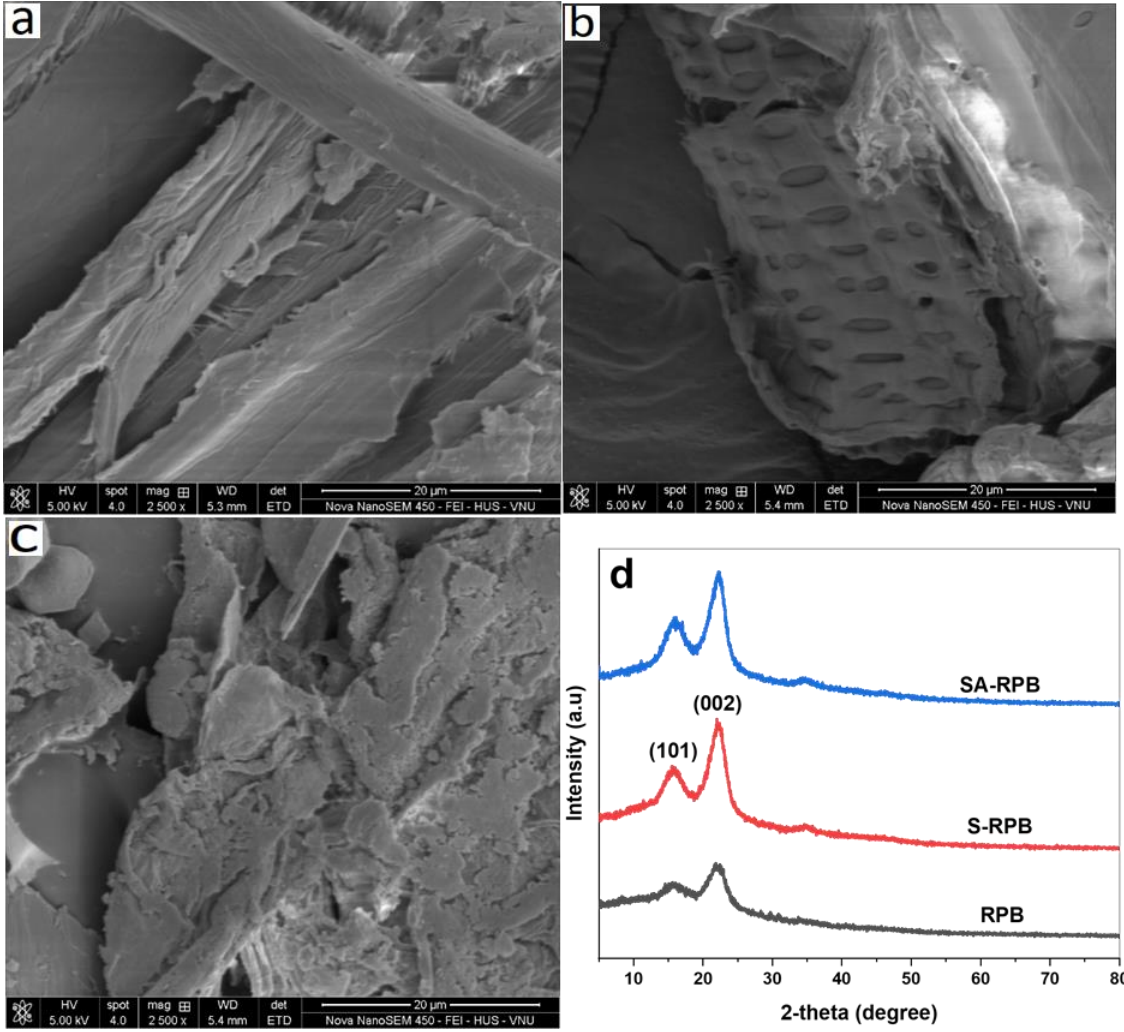


Figure 1: Morphology and crystallization of samples. SEM images of (a) RPB, (b) S-RPB, and (c) SA-RPB; (d) XRD patterns of RPB, S-RPB, and SA-RPB samples

The functional groups on the adsorbent surfaces with differences in intensities of the observed peaks during *P. australis* biomass modification were analyzed using FTIR (Figure 2). Absorption bands corresponding to functional groups were determined according to Reddy [46]. A broad peak of approximately 3321 cm<sup>-1</sup> corresponded to the stretching vibration of the hydroxyl groups (–OH) for cellulose, hemicellulose, and lignin, whereas the 2918 cm<sup>-1</sup> band indicated the presence of C–H stretching vibrations of methyl and methylene. After the raw material was modified with NaOH and NaOH followed with citric acid, the stretching vibration bands of OH shifted to 3443 and 3438 cm<sup>-1</sup>, respectively. The band at 1734 cm<sup>-1</sup> could be attributed to the C=O bond stretching of acetyl ester groups in hemicellulose, lignin, or both.

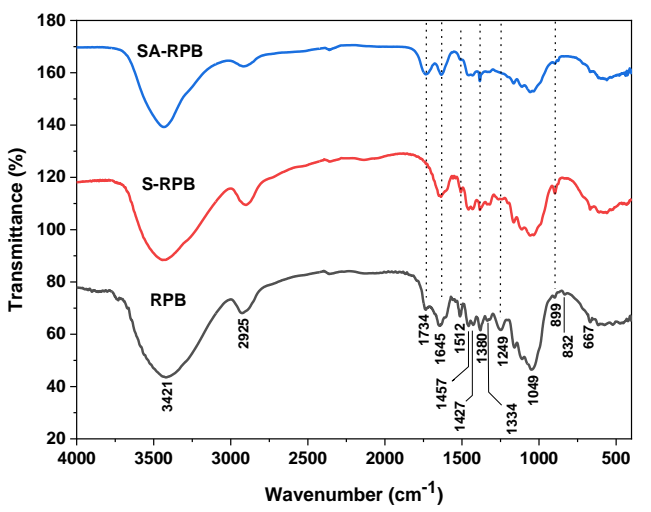


Figure 2: FTIR spectra of RPB, S-RPB and SA-RPB samples

This absorption peak was absent from the FTIR spectrum of the S-RPB sample (Figure 2 and Table 7) after alkaline treatment because of the removal of hemicellulose and lignin through a process called de-esterification. Moreover, C=O bond stretching was observed after treatment with NaOH and citric acid, owing to the esterification reaction. The band at 1645 cm<sup>-1</sup> could be attributed to -COO- stretching of carboxylate groups with the aromatic ring. The band at approximately 1512 cm<sup>-1</sup> was associated with C = C stretching vibrations in aromatic rings of lignin, whereas the band at 1427 cm<sup>-1</sup> was attributed to the C-H bond deformation of lignin. The peak intensities at 1457 and 1380 cm-1 reflected C-H symmetric and asymmetric deformations of cellulose, respectively. The appearance of peaks at 1334 and 1327 cm<sup>-1</sup> could be attributed to the –OH bending vibration in C–OH and C1-O vibrations in S derivative vibrations of cellulose, respectively. The signal at 1249 cm<sup>-1</sup> corresponded to the -COO vibration of acetyl groups in hemicellulose and lignin [20, 47]. The absorption peaks at 1159 and 1111 cm<sup>-1</sup> were attributed to C-O-C antisymmetric and anhydroglucose ring vibrations, respectively, whereas the band at 1049 cm<sup>-1</sup> corresponded to C-O stretching vibrations of cellulose, hemicellulose, and lignin [48]. A band at 899 cm<sup>-1</sup> corresponds to C–H rocking vibrations of cellulose [49]. The intensities of these parts of S-RPB and SA-RPB decreased, owing to the removal of lignin. The weak absorption peaks of 832– 400 cm<sup>-1</sup> were probably related to C≡H and C=H bending in aromatic rings [40], C-H bending, and C-O stretching [50]. The FTIR results indicated abundant functional groups of -OH, -COOH, and -COO- on the adsorbent surfaces.

### 3.2 pH<sub>PZC</sub> determination

The differences in the pH<sub>PZC</sub> of RPB, S-RPB, and SA-RPB are shown in Figure 3(a). The raw *P. australis* biomass had a pH<sub>PZC</sub> of 6.72, also obtained in a previous study [27].

Table 7: FTIR spectral characteristics of MB and SA-RPB before and after MB adsorption

MB		SA-RPB				
	Waxanumban		Wavenumber			
Vibration	Wavenumber (cm <sup>-1</sup> )	Vibration	Before Adsorption (cm <sup>-1</sup> )	After Adsorption (cm <sup>-1</sup> )		
O-H or N-H stretching	3424	-OH stretching	3438	3427		
-CH <sub>3</sub> stretching	2939	C-H stretching vibration	2917	2915		
C=N-C group	2360	–COOH stretching vibration	1735	1734		
=N <sup>+</sup> (CH <sub>3</sub> ) <sub>2</sub> stretching	1661	-COO stretching of carboxylate groups with an aromatic ring	1633	1601		
C=N (and C=C) stretching in heterocycle	1599	C=C stretching vibrations in aromatic rings	1506	-		
C-H deformation in benzene ring	1492	C–H deformation in aromatic rings	1456	1489		
C-N in heterocycle	1396	C=C stretching vibrations in aromatic rings	1431	1447		
C–N bonds connected with benzene ring	1356	C-H asymmetric deformation	1384	1385		
N-CH <sub>3</sub> stretching	1340	-OH bending vibration in C-OH	1334	1355		
		C1-O vibrations in S derivatives	1321	1335		
Ar-N deformation vibration	1252		-	1249		
C=S stretching vibration	1183	C–O–C antisymmetric vibrations	1165	1164		
C–S stretching vibration	1142	Anhydroglucose ring vibration	1111	1109		
C–N stretching vibration	1066;	C-O stretching vibration in cellulose,	1057;	1056;		
C-14 successing vibration	1038	hemicellulose, and lignin	1035	1034		
C–H axial deformation in aromataic rings	950- 669	C-H rocking vibrations	898	897		
C-S and C-N stretching	616-449	C-H bending in aromatic rings	875-500	875-500		

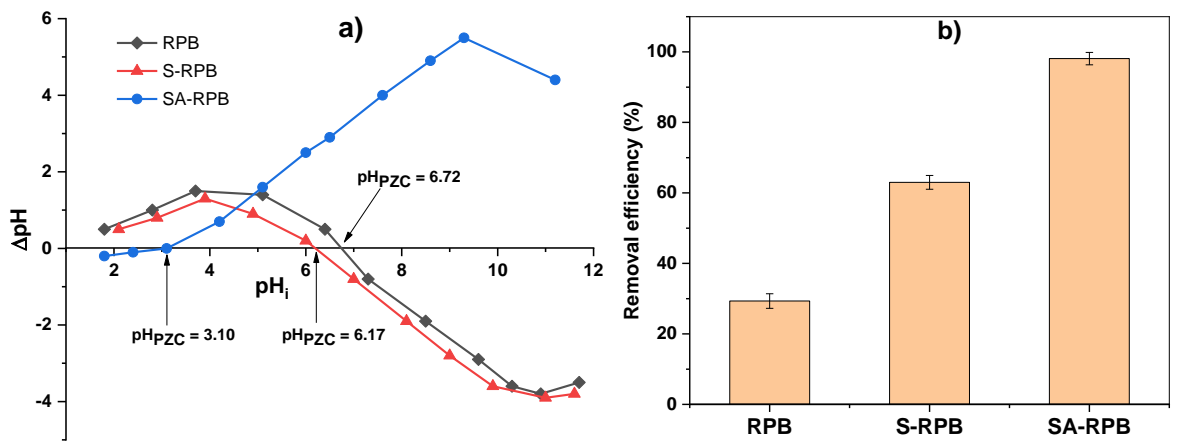


Figure 3: (a) Plots of point of zero charges of RPB, S-RPB, and SA-RPB and (b) percentage removal efficiency values for MB on RPB, S-RPB, and SA-RPB samples

The pH<sub>PZC</sub> level slightly decreased after treatment with NaOH, possibly because of de-esterification and the removal of a part of hemicellulose and ligin [51]. The pH<sub>PZC</sub> value of SA-RPB was significantly lower than those of RPB and S-RPB, which could be attributed to the esterification reaction of hydroxyl on the raw material surface with the carboxyl group of citric acid to increase the carboxyl group on its surface [20, 52]. Absorbents with pH values lower than pH<sub>PZC</sub> absorb compounds with a positive surface charge [53]. The MB dye with a molecular diameter of 0.8 nm [54] was smaller than the pore diameter of SA-RPB (15.97 nm, Table 2); hence, MB could easily penetrate the SA-RPB pore structure. The batch adsorption test results showed that the removal efficiency of SA-RPB adsorbent was 98.11±1.76%, about 35.1 and 68.8% higher than that of RPB and S-RPB, respectively (Figure 3(b)). Therefore, SA-RPB was used for other experiments.

#### 3.3 Batch adsorption

# 3.3.1 Effect of adsorbent dosage

For this experiment, the effects of the adsorbent dose (SA-RPB) on MB adsorption were examined. Figure 4 shows that an increase in the adsorbent mass from 0.4 to 1.0 g/L improved the MB removal rate because of the increase in the sites available for absorption. However, the adsorption did not statistically increase at adsorbent doses higher than 1.0 g/L. The adsorption tended to an equilibrium when the adsorbent mass reached a particular value, possibly because the available number of MB dye molecules in the solution was insufficient to combine with all effective adsorption sites on the adsorbent.

# 3.3.2 Effects of contact time, temperature, and adsorption kinetics

The effect of contact time on MB removal using the SA-RPB adsorbent is depicted in Figure 5. The adsorption isotherms at three temperatures were not statistically different. The absorption sharply increased within 20 min at the initial stage and then attained equilibrium after 60 min at all temperatures. This phenomenon was observed in previous studies using modified plant materials to remove MB [55, 56]. The decrease in the number of vacant sites and the lack of available active sites of the adsorbent decreased the adsorption rate and slowed down the equilibrium [56].

Two kinetic models (pseudo-first-order and pseudo-secondorder models) were used to determine the adsorption rate and analyze the kinetic data. The calculated correlation coefficients ( $R^2$ ) and other data are listed in Table 3. The  $q_{e,cal}$  and  $q_{e,exp}$  values for each model at different temperatures were not statistically different, whereas  $k_1$  and  $k_2$  tended to increase at higher temperatures, indicating that the adsorption kinetics was more rapid at higher temperatures.

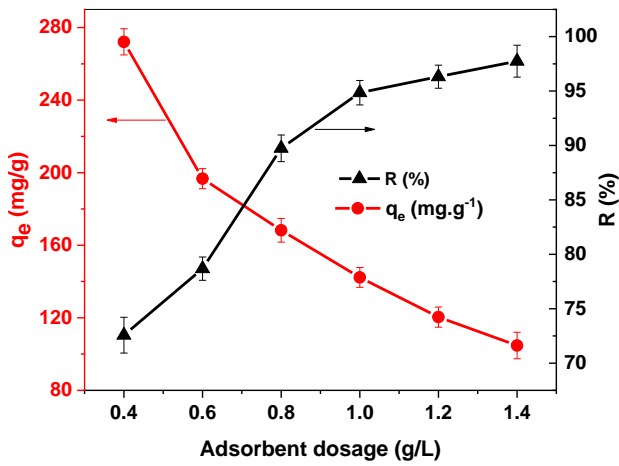


Figure 4: Effect of SA-RPB dosages on equilibrium adsorption capacity  $(q_e, \text{mg/g})$  and removal efficiency of MB (R, %). The tests were conducted for 105 min using 150 mg/L MB at pH of 6.5

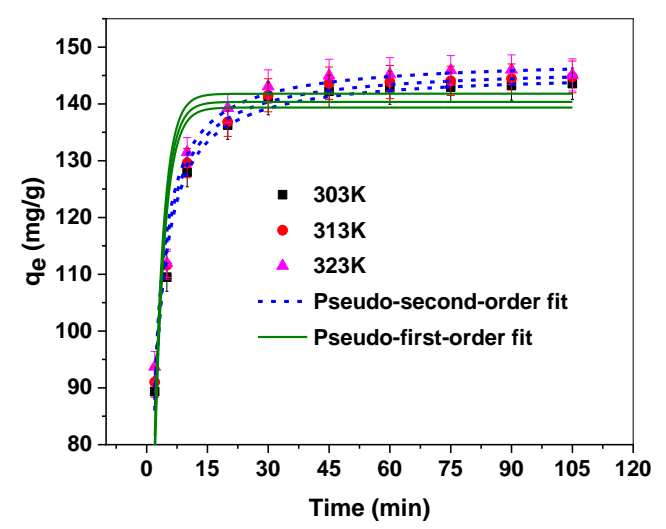


Figure 5: Pseudo-first and pseudo-second-order kinetics for MB adsorption onto SA-RPB at different temperatures. The tests were conducted using 1.0 g/L SA-RPB and 150 mg/L MB at pH of 6.5

Table 3: Kinetic parameters for MB adsorption onto SA-RPB at different temperatures

Temperature	$q_{e,exp}$		First-order kinetic model			Seco	ond-order kinet	ic model	
( <b>K</b> )	(mg/g)	$\overline{k_1  (\text{min}^{-1})}$	q <sub>e,cal</sub> (mg/g)	$R^2$	$\chi^2$	k <sub>2</sub> (g/mg.min)	q <sub>e,cal</sub> (mg/g)	$R^2$	$\chi^2$
303	143.56	0.4047	139.36	0.807	4.084	0.0049	145.64	0.987	0.340
313	144.75	0.4192	140.35	0.849	3.841	0.0051	146.58	0.989	0.281
323	145.11	0.4275	141.79	0.828	4.241	0.0052	147.93	0.981	0.467

The second-order kinetic model of MB adsorption onto SA-RPB fitted precisely with high correlation coefficients ( $R^2 > 0.98$ ). Moreover, slight differences between the calculated data ( $q_{e,cal}$ ) and experimental data ( $q_{e,exp}$ ) and the low  $\chi^2$  values of the second-order kinetic model indicated the optimum adsorption at the equilibrium of the kinetic model. The second-order kinetic model satisfactorily simulates MB adsorption onto modified cellulose fibers of P. australis [26, 27].

# 3.3.3 Effects of initial MB concentration and adsorption isotherms

The removal efficiency of MB using SA-RPB depended on the chemical concentration (Figure 6(a)). The removal rate rapidly increased from 125 to 250 mg/L MB concentrations and gradually increased at higher concentrations. More than 94% MB was absorbed using 125 and 150 mg/L concentrations, and the dye equilibrium adsorption capacity ( $q_e$ ) decreased at higher concentrations (Figure 6(a)). The adsorption isotherms, which revealed the interactive behaviors between the adsorbate and adsorbent at liquid–solid interfaces, were analyzed. The Langmuir,

Freundlich, Dubinin-Radushkevitch, and Temkin models simulated the MB adsorption onto SA-RPB. The nonlinear plots of the isotherm models at different temperatures are shown in Figure 6(b)–(d), and their corresponding parameters are listed in Table 4.  $R^2$  and  $\chi^2$  were used as indicators to analyze the adsorption at equilibrium. The Langmuir model yielded the best fit because of its higher  $R^2$  and lower  $\chi^2$  than those of other models. The Langmuir isotherm model showed the homogeneous nature of the adsorbent surface and the monolayer cover of dye molecules formed at the outer surface of the adsorbents under NaOH and citric acid treatment. The  $R_L$  values of the Langmuir isotherm indicated that the fundamental features were higher than 0 and less than 1.0; thus, the adsorption was favorable within the evaluated concentration range [57]. R<sub>L</sub> increased with temperatures, suggesting favorable adsorption of the MB onto the SA-RPB under the conditions. For the Freundlich model, the 1/n values (Table 4) were within the range of 0.1 < 1/n < 1.0, signifying physisorption mechanism, and the adsorption process was considered favorable, rapid, and effective [58].

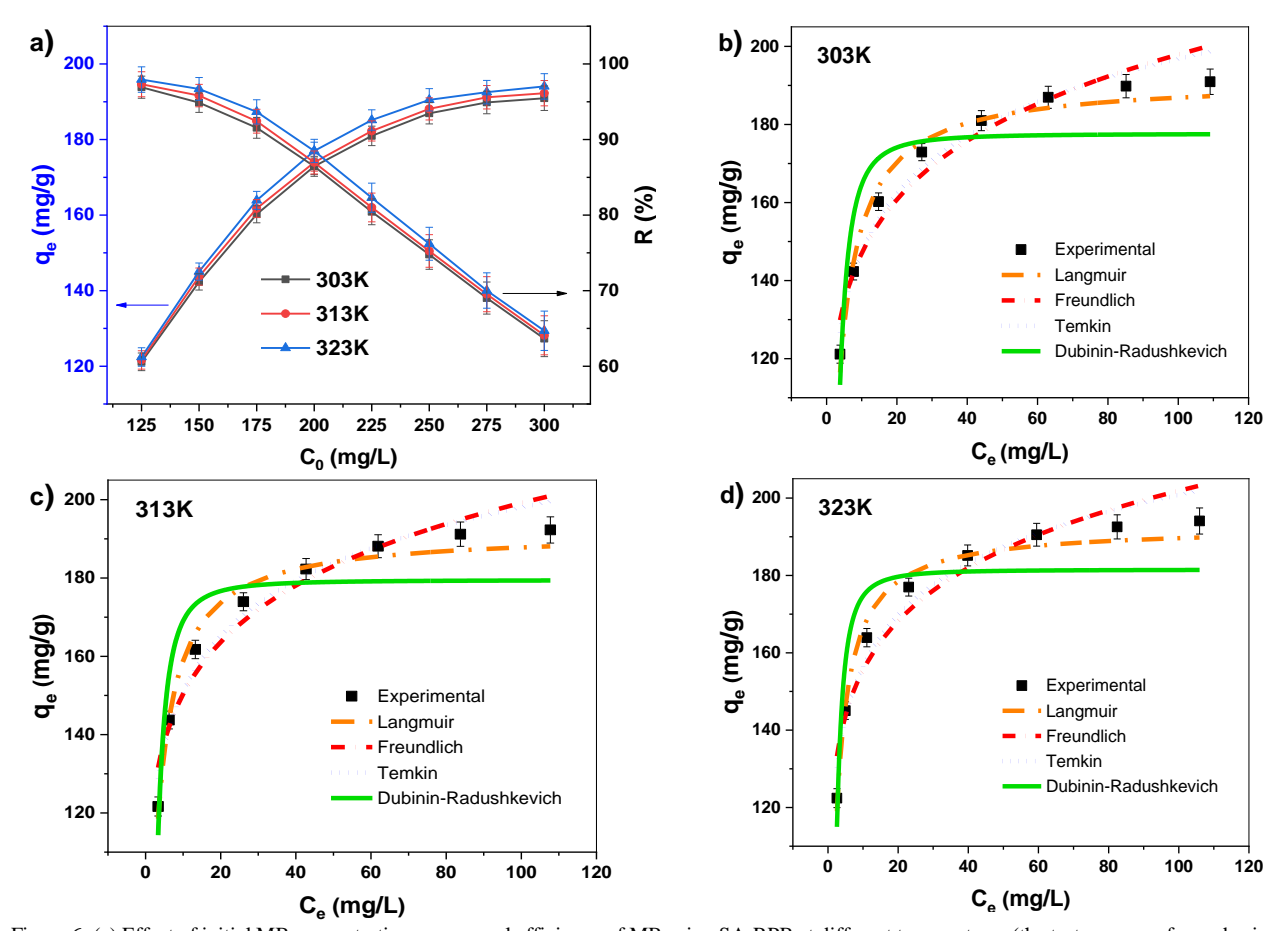


Figure 6: (a) Effect of initial MB concentration on removal efficiency of MB using SA-RPB at different temperatures (the tests were performed using 1.0 g/L SA-RPB and pH of 6.5); (b)–(d) Analyses of MB adsorption isotherm using SA-RPB based on Langmuir, Freundlich, Temkin, and Dubinin–Radushkevich isotherm models at 303, 313, and 323 K. The experiments were conducted using 1.0 g/L SA-RPB at 150 mg/L MB concentration and pH of 6.5

Table 4: Isotherm parameters for MB adsorption onto SA-RPB at different temperatures

Tomporeture				muir isotherm			Fre	eundlich isot	herm	
Temperature (K)	$q_{\rm e,exp}$ (mg/g)	$q_{\text{max}}$ (mg/g)	$K_{\rm L}({ m L/mg})$	$R_{ m L}$	$R^2(L)$	$\chi^2(L)$	$K_F$ (mg/g.(L/mg) <sup>1</sup>	$^{/n})^{n_F}$	$R^2(F)$	$\chi^2(F)$
303	190.94	191.49	0.404	0.0082	0.981	0.548	109.15	7.739	0.946	99.505
313	192.27	191.68	0.484	0.0068	0.983	0.482	113.53	8.194	0.946	97.580
323	194.07	192.64	0.629	0.0053	0.983	0.491	119.74	8.815	0.933	96.707
Temperature	a (mala)	Dubinin-Rac		Dubinin-Radushkevitch isotherm			Temkin isotherm			
( <b>K</b> )	$q_{\rm e,exp}$ (mg/g)	$q_{DR}$ (mg/g)	E (kJ/mol)	$K_{DR}$ (mol <sup>2</sup> /kJ <sup>2</sup>	$R^2(D)$	$\chi^2(D)$	$A_T(L/mg)$	$B_T(J/mol)$	$R^2(T)$	$\chi^2(T)$
303	190.94	177.62	0.615	$-1.32 \times 10^{-6}$	0.817	5.135	95.656	21.470	0.970	0.867
313	192.27	179.47	0.716	$-0.97 \times 10^{-6}$	0.846	4.414	163.32	20.414	0.967	0.980
323	194.07	181.48	0.924	$-0.58 \times 10^{-6}$	0.847	4.441	336.91	19.263	0.959	1.244

Table 5: Comparison of adsorption capacities of different MB adsorbents

Adsorbent	Temperature (K)	pН	q <sub>max</sub> (mg/g)	References
P. australis treated with NaOH and citric acid	303	6.5	191.49	Present study
P. australis treated with NaOH	298	7.0	54.9	Kankılıç & Metin 2016
Raw P. australis	298	6.5	22.7	Kankılıç et al. 2016
P. australis treated with organic compounds	298	6.5	46.8	Kankılıç et al. 2016
Raw Tunisian P. australis	298	8.0	41.2	Dallel et al. 2018
Lawny grass treated with citric acid	298	5.7	301.1	Chen et al. 2011
Peach stones modified with citric acid	303	6.0	178.25	Yan et al. 2018
Peanut shell modified with citric acid	303	10.0	120.48	Wang et al. 2015
Activated carbon	303	7	81.20	Yusop et al. 2021

Table 6: Thermodynamic parameters for MB adsorption onto SA-RPB

E <sub>a</sub> (kJ/mol)	A (g/mg.min)	Temperature (K)	ΔG <sup>0</sup> (kJ/mol)	ΔH <sup>0</sup> (kJ/mol)	ΔS <sup>0</sup> (kJ/mol.K)
		303	-28.63		
2.242	0.012	313	-30.18	16.82	0.155
		323	-31.73		

The obtained adsorbent modified with NaOH and citric acid exhibited effective MB removal with the maximum adsorption capacity of 191.49 mg/g at 150 mg/L MB concentration. This value is higher than those obtained in other studies using modified *P. australis* biomass [26, 27, 58] and other modified plant materials listed in Table 5. For example, Kankılıç *et al.* (2016) reported that the maximum adsorption capacity of cellulose microfibrils of *P. australis* modified with NaOH was 54.9 mg/g at 400 mg/L. The treatment with citric acid increased the adsorption ability in this study.

# 3.3.4 Adsorption thermodynamics

The thermodynamic study evaluates the feasibility of the adsorption process. The Arrhenius equation (Eq. (18)) was used to calculate the effect of temperature on the velocity of a chemical reaction, which is the basis for all predictive expressions of reaction-rate constants.

$$lnk_2 = lnA - \frac{E_a}{RT} \tag{18}$$

In Eq. (18), A (g/mg·min) is the pre-exponential factor,  $E_a$  (kJ/mol) is the activation energy of the adsorption, R (8.314 J/mol.K) is the gas constant, and T (K) is the absolute temperature. Plots of  $\ln K_2$  versus 1/T and  $\ln K_L$  versus 1/T were straight lines with  $R^2$  values of 0.99 and 0.98, respectively, from which  $E_a$  and A values were calculated (Table 6). The low values of activation energy (< 42 kJ/mol) obtained in this study indicated a diffusion-controlled process and a physisorption mechanism [59]. The negative values of  $\Delta G^0$  at all temperatures revealed that the adsorption process was feasible and spontaneous. The obtained  $\Delta H^o$  was positive, showing the endothermic nature of adsorption. The positive  $\Delta S^o$  suggested increased randomness of the solid–liquid and adsorption medium interface during adsorption.

#### 3.3.5 Effect of initial pH

The increase in pH from 1.0 to 6.5 significantly increased the adsorption, and the adsorption rates were not significantly changed at a higher pH (Figure 7). The effect of pH on the MB removal efficiency could be attributed to the characteristics of the functional groups on the surface and isoelectric point pH<sub>PZC</sub> of the SA-RPB adsorbent. The isoelectric point pH<sub>PZC</sub> value of SA-RPB, determined using the drift pH method, was 3.1 (Figure 3(a)). The hydroxyl (-OH) and carboxyl (-COOH) groups were dominant on the SA-RPB surface, which was deprotonated and became less charged, that is  $pH_{PZC} < 3.1$  [60]. When the initial pH ( $pH_{in}$ ) was lower than pH<sub>PZC</sub> (3.1), the adsorbent surface was protonated and became more positive [60]. In this case, the SA-RPB surface exhibited an electrostatic repulsion between the SA-RPB surface and the MB-N<sup>+</sup> cation in the solution, leading to poor adsorption efficiency [61]. In contrast, when the pH value was lower than pH<sub>PZC</sub>, the functional groups on the SA-RPB surface were deprotonated and became more negative; this phenomenon induced electrostatic attraction to MB-N+, increasing the removal efficiency [61].

### 3.3.6 Possible mechanism of MB adsorption onto SA-RPB

Dye adsorption involves interactions between the adsorbent and the adsorbate in the solution. Based on the result ( $\Delta H^o = 16.82$  kJ/mol), adsorption was mainly induced by electrostatic and/or hydrogen bond forces [62]. At a pH < 3.1 (pH<sub>PZC</sub> of SA-RPB), the protonated adsorbent surface became positively charged (Figure 3(a)). Therefore, the MB–N<sup>+</sup> adsorption was mainly attributed to the physical interaction caused by capillary diffusion and weak hydrogen bonds. The surface of the negatively charged adsorbent electrostatically interacted with MB–N<sup>+</sup> at pH > 3.1, improving the adsorption efficiency. The MB adsorption efficiency of the SA-RPB reached the maximum value at the initial pH of the MB

solution (6.5); hence, this pH value was selected to evaluate the adsorption mechanism.

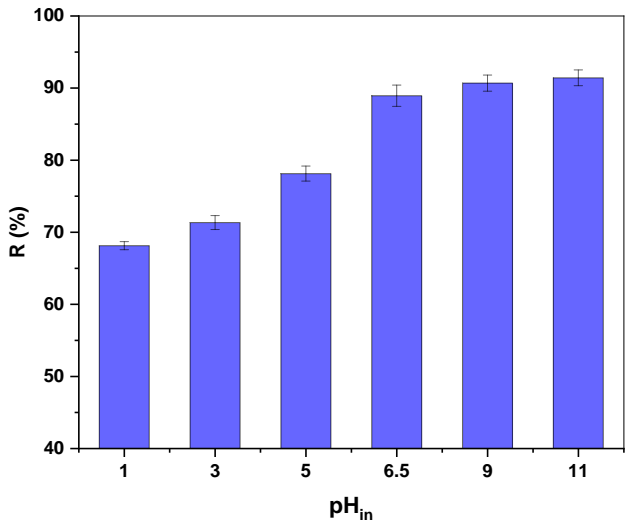


Figure 7: Effect of initial pH value on MB adsorption onto SA-RPB. The tests were performed using 1.0 g/L SA-RPB at 150 mg/L MB concentration

The FTIR analysis plots showed the spectra of the MB, SA-RPB, and SA-RPB after MB adsorption and were used to describe the adsorption mechanisms. From the spectra peaks (Figure 8), vibrations were revealed (Table 7). Based on the wavenumbers, it was inferred that pure MB had functional groups, that is, -OH, C=C, C=N, C=N<sup>+</sup>, C-N, C=S, C-S, and C-H [63, 64]. The variations in peak positions of the functional groups and the strength of the SA-RPB dye complex indicated MB adsorption onto the SA-RPB surface. The differences in the wavenumbers for

C–H deformation in the benzene ring, C–N in the heterocycle and C–N bonds connected with benzene ring in the MB, C–H aromatic rings, C=C stretching vibrations in aromatic rings, and C– H asymmetric deformation in the SA-RPB and SA-RPB dye complex (Table 7) corresponded to MB attachment to the surface of the adsorbent by  $\pi$ – $\pi$  stacking between the aromatic backbone of the MB and SA-RPB [50, 63]. This interaction was evident with absorption peaks of MB and SA-RPB at 1599 and 1506 cm<sup>-1</sup>, respectively, disappearing in the SA-RPB dye complex. Furthermore, the SA-RPB peak at 897 cm<sup>-1</sup> after MB adsorption (Figure 9), attributed to the bending vibration of C–H in the aromatic ring, increased to a higher intensity than the SA-RPB sample before MB adsorption.

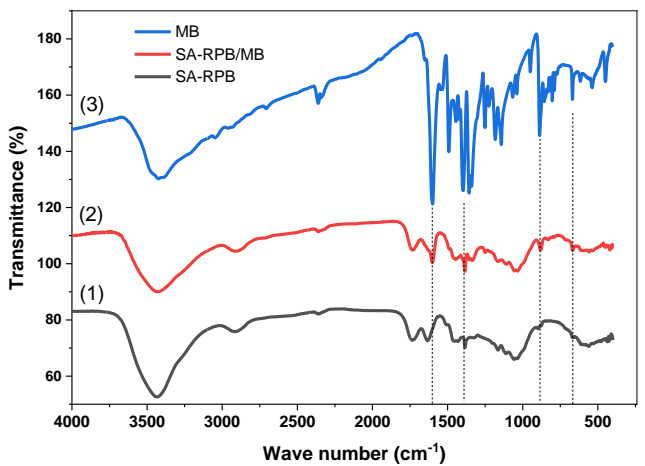
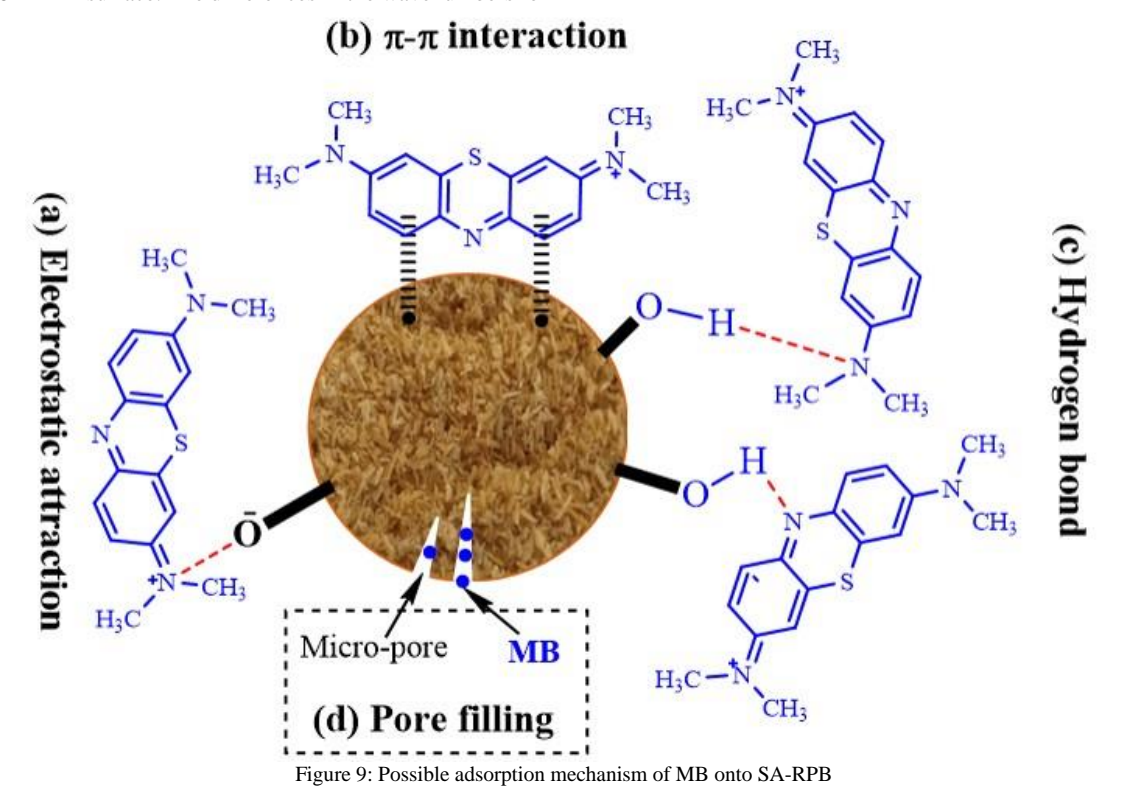


Figure 8: FTIR spectra of SA-RPB (1) before and (2) after MB adsorption and (3) pure MB



The peak ranges of 1340–1000 cm<sup>-1</sup> of SA-RPB with oxygenrich functional groups shifted, suggesting the formation of

hydrogen bonds between SA-RPB and MB molecules. The band shifts occurred as N-CH<sub>3</sub> stretching, Ar-N deformation vibration,

C=S stretching vibration, and C-S stretching vibration. These phenomena indicated that N in the  $-N(CH_3)_2$  and Ar-N groups and S in the C=S and C-S groups might have been used as the hydrogen-bonding acceptor and formed intramolecular hydrogen bonding with the hydrogen atom of the -OH and -COOH groups on the adsorbent surface [63]. Hydrogen atoms in the functional groups of SA-RPB could also form hydrogen bonds with N and S in the functional groups of MB. In addition, the SA-RPB dye complex had a new absorption peak at 1249 cm<sup>-1</sup>, owing to the Ar-N deformation vibration of the MB molecule; this verified MB adsorption onto the SA-RPB surface. Based on the above analysis results, the adsorption efficiency of the MB onto the SA-RPB was attributed to four possible adsorption mechanisms: electrostatic interaction, hydrogen bonding,  $\pi$ - $\pi$  stacking interaction, and filling of pores between the MB and SA-RPB (Figure 9).

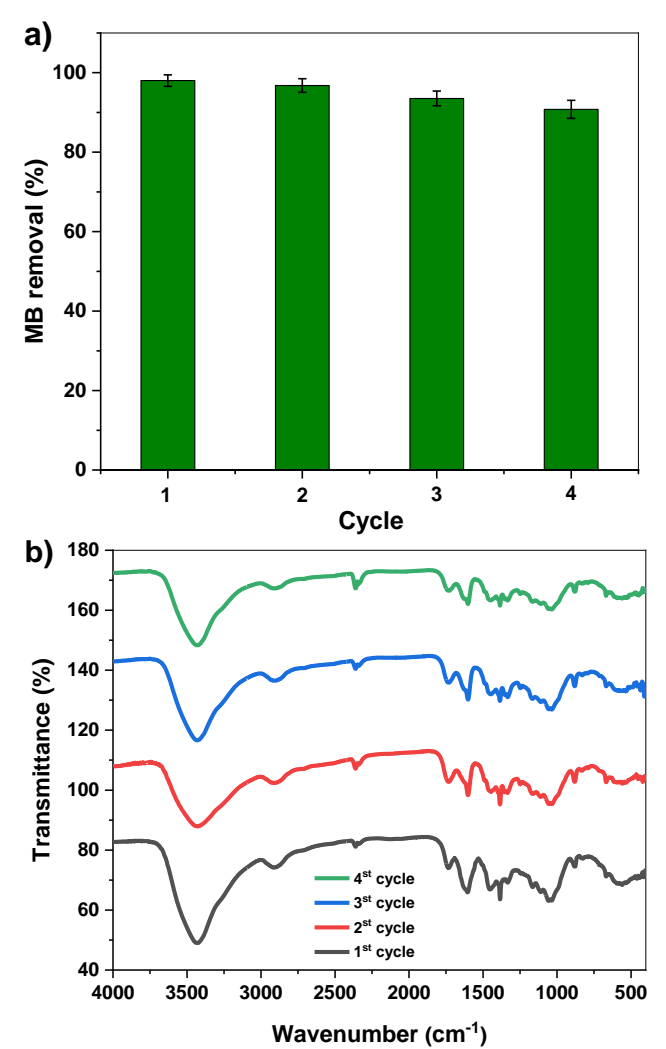


Figure 10: (a) Removal efficiency of MB onto SA-RPB in successive desorption—adsorption cycles; (b) FTIR spectra of SA-RPB after four desorption—adsorption cycles. The tests were conducted using 1.0 g/L SA-RPB at 150 mg/L MB concentration and pH of 6.5

# 3.4 Reusability

The reusable efficiency of an adsorbent for wastewater treatment is a critical factor for economic purposes. The regeneration results showed that the adsorption capacity decreased by approximately 7% after four desorption—adsorption cycles compared with the first batch experiment (Figure 10(a)). Additionally, FTIR spectra of adsorbents showed similar spectra

after four cycles (Figure 10(b)), indicating the stability of the adsorbent during the adsorption process.

#### 4 Conclusion

This study demonstrates that chemically modified P. australis biomass can be used as an adsorbent for removing MB dye from aqueous solutions. The batch adsorption test results showed that the material treated with NaOH and citric acid increased the removal efficiency by about 35.1 and 68.8% compared with the raw material and the raw material modified with only NaOH, respectively. The initial pH of the solution, the adsorbent dosage, contact time, and initial MB concentrations significantly influenced the adsorption rates of SA-RPB. SEM, FTIR, and BET analysis indicated significant modification in the structure after chemical treatments. Moreover, the calculated adsorption energy indicated that MB adsorption onto SA-RPB occurred through physical interactions at different temperatures when the removal process was endothermic and spontaneous. The maximum adsorption capacity of SA-RPB for MB was 191.49 mg/g, which was slightly decreased after four desorption-adsorption cycles. The overall results of this study suggested that the SA-RPB can be a favorable adsorbent for treating MB in wastewater.

# Acknowledgements

This research is supported by the project SPD2020.01.05. The authors are thankful to Dong Thap University for providing the instrumental facility and financial support. We are also thankful anonymous reviewers and editors whose suggestions helped improve and clarify this manuscript.

# Ethical issue

Authors are aware of and comply with, best practices in publication ethics specifically with regard to authorship (avoidance of guest authorship), dual submission, manipulation of figures, competing interests, and compliance with policies on research ethics. Authors adhere to publication requirements that submitted work is original and has not been published elsewhere in any language. Also, all procedures performed in studies involving human participants were in accordance with the ethical standards of the institutional and/or national research committee and with the 1964 Helsinki declaration and its later amendments or comparable ethical standards. All procedures performed in this study involving animals were following the ethical standards of the institution or practice at which the studies were conducted.

# **Competing interests**

The authors declare that no conflict of interest would prejudice the impartiality of this scientific work.

# **Authors' contribution**

All authors of this study have a complete contribution for data collection, data analyses, and manuscript writing.

# References

- Yao Y, Xu F, Chen M, Xu Z, Zhu Z. Adsorption behavior of methylene blue on carbon nanotubes. Bioresour Technol. 2010, 101(9), 3040-3046.
- [2] Meili L, Lins PVS, Costa MT, Almeida RL, Abud AKS, Soletti JI, Dotto GL, Tanabe, EH, Sellaoui L, Carvalho SHV, Erto A. Adsorption of methylene blue on agroindustrial wastes, Experimental investigation and phenomenological modelling. Prog Biophys Mol Biol. 2019, 141, 60-71.
- [3] Nasuha N, Hameed BH, Din AT. Rejected tea as a potential low-cost adsorbent for the removal of methylene blue. J Hazard Mater. 2010, 175(1-3), 126-132.

- [4] Ahmed MJ, Dhedan SK. Equilibrium isotherms and kinetics modeling of methylene blue adsorption on agricultural wastes-based activated carbons. Fluid Phase Equilibria. 2012, 317, 9-14.
- [5] Lahkimi A, Oturan MA, Oturan N, Chaouch M. Removal of textile dyes from water by the electro-Fenton process. Environ Chem Lett. 2006, 5(1), 35-39.
- [6] Panizza M, Barbucci A, Ricotti R, Cerisola G. Electrochemical degradation of methylene blue. Sep Purif Technol. 2007, 54(3), 382-387
- [7] Nataraj SK, Hosamani KM, Aminabhavi TM. Nanofiltration and reverse osmosis thin film composite membrane module for the removal of dye and salts from the simulated mixtures. Desalination. 2009, 249(1), 12-17.
- [8] Gulshan F, Yanagida S, Kameshima Y, Isobe T, Nakajima A, Okada K. Various factors affecting photodecomposition of methylene blue by iron-oxides in an oxalate solution. Water Res. 2010, 44(9), 2876-2884.
- [9] Yeap KL, Teng TT, Poh BT, Morad N, Lee KE. Preparation and characterization of coagulation/flocculation behavior of a novel inorganic-organic hybrid polymer for reactive and disperse dyes removal. Chem Eng Sci. 2014, 243, 305-314.
- [10] Soniya M, Muthuraman G. Comparative study between liquid—liquid extraction and bulk liquid membrane for the removal and recovery of methylene blue from wastewater. Ind Eng Chem. 2015, 30, 266-273.
- [11] Khaksar M, Boghaei DM, Amini M. Synthesis, structural characterization and reactivity of manganese tungstate nanoparticles in the oxidative degradation of methylene blue. Comptes Rendus Chimie. 2015, 18(2), 199-203.
- [12] Mbacké MK, Kane C, Diallo NO, Diop CM, Chauvet F, Comtat M, Tzedakis T. Electrocoagulation process applied on pollutants treatment-experimental optimization and fundamental investigation of the crystal violet dye removal. J Environ Chem Eng. 2016, 4(4), 4001-4011
- [13] Ahlawat W, Kataria N, Dilbaghi N, Hassan AA, Kumar S, Kim KH. Carbonaceous nanomaterials as effective and efficient platforms for removal of dyes from aqueous systems. Environ Res. 2020, 181, 108004
- [14] Hoc Thang N, Sy Khang D, Duy Hai T, Thi Nga D, Dinh Tuan P. Methylene blue adsorption mechanism of activated carbon synthesised from cashew nut shells. RSC Advances. 2021, 11(43), 26563-26570.
- [15] Yusop MFM, Ahmad MA, Rosli NA, Manaf MEA. Adsorption of cationic methylene blue dye using microwave-assisted activated carbon derived from acacia wood, optimization and batch studies. Arabian Journal of Chemistry. 2021, 14(6), 103122.
- [16] Marrakchi F, Ahmed MJ, Khanday WA, Asif M, Hameed BH. Mesoporous-activated carbon prepared from chitosan flakes via single-step sodium hydroxide activation for the adsorption of methylene blue. Int J Biol Macromol. 2017, 98, 233-239.
- [17] Jawad AH, Hanani Mamat NF, Fauzi Abdullah M, Ismail K. Adsorption of methylene blue onto acid-treated mango peels, kinetic, equilibrium and thermodynamic. Desalin Water Treat. 2016, 59, 210-219.
- [18] Manikandan G, Kumar PS, Saravanan A. Modelling and analysis on the removal of methylene blue dye from aqueous solution using physically/chemically modified *Ceiba pentandra* seeds. J. Ind Eng Chem. 2018, 62, 446-461.
- [19] Georgin J, Marques BS, Peres EC, Allasia D, Dotto GL. Biosorption of cationic dyes by *Para chestnut* husk (*Bertholletia excelsa*). Water Sci Technol. 2018, 77(5-6), 1612-1621.
- [20] Yan J, Lan G, Qiu H, Chen C, Liu Y, Du G, Zhang J. Adsorption of heavy metals and methylene blue from aqueous solution with citric acid modified peach stone. Sep Sci Technol. 2018, 53(11), 1678-1688.
- [21] Jawad AH, Razuan R, Appaturi JN, Wilson LD. Adsorption and mechanism study for methylene blue dye removal with carbonized watermelon (*Citrullus lanatus*) rind prepared via one-step liquid phase H<sub>2</sub>SO<sub>4</sub> activation. Surf Interfaces. 2019, 16, 76-84.
- [22] Sebeia N, Jabli M, Ghith A, El Ghoul Y, Alminderej FM. *Populus tremula, Nerium oleander* and *Pergularia tomentosa* seed fibers as sources of cellulose and lignin for the bio-sorption of methylene blue. Int J Biol Macromol. 2019. 121, 655-665.
- [23] Ben Jeddou K, Bouaziz F, Ben Taheur F, Nouri-Ellouz O, Ellouz-Ghorbel R, Ellouz-Chaabouni S. Adsorptive removal of direct red 80 and methylene blue from aqueous solution by potato peels, a comparison of anionic and cationic dyes. Water Sci Technol. 2021, 83(6), 1384-1398.

- [24] Engloner AI. Structure, growth dynamics and biomass of reed (*Phragmites australis*) a review. Morphol. 2009, 204(5), 331-346.
- [25] Březinová T, Vymazal J. Competition of *Phragmites australis* and *Phalaris arundinacea* in constructed wetlands with horizontal subsurface flow does it affect BOD5, COD and TSS removal?. Ecol Eng. 2014, 73, 53-57.
- [26] Kankılıç GB, Metin AÜ. Phragmites australis as a new cellulose source, extraction, characterization and adsorption of methylene blue. J Mol Liq. 2020, 312, 113313.
- [27] Dallel R, Kesraoui A, Seffen M. Biosorption of cationic dye onto Phragmites australis fibers, Characterization and mechanism. J Environ Chem Eng. 2018, 6(6), 7247-7256.
- [28] Chen L, Ramadan A, Lü L, Shao W, Luo F, Chen J. Biosorption of methylene blue from aqueous solution using lawny grass modified with citric acid. J Chem Eng Data. 2011, 56(8), 3392-3399.
- [29] Wang P, Ma Q, Hu D, Wang L. Adsorption of methylene blue by a low-cost biosorbent, citric acid modified peanut shell. Desalin Water Treat. 2015, 57(22), 10261-10269.
- [30] Sluiter A. HB, Ruiz R., Scarlata C., Sluiter J., Templeton D., and Crocker D. Determination of structural carbohydrates and lignin in biomass, laboratory analytical procedure (LAP), National Renewable Energy Laboratory Golden Co., 2008.
- [31] Danish M, Ahmad T, Majeed S, Ahmad M, Ziyang L, Pin Z., Shakeel Iqubal SM. Use of banana trunk waste as activated carbon in scavenging methylene blue dye: kinetic, thermodynamic, and isotherm studies Bioresour Technol Rep. 2018, 3, 127–137.
- [32] Lagergren S. About the theory of so called adsorption of soluble substances, kungliga Svenska Vetenskapsakademiens. Handlingar Band, 1898, 24(4), 1-39.
- [33] Ho YS, McKay G. Pseudo-second-order model for sorption processes. Process Biochem. 1999, 34, 451-465.
- [34] Mouni L, Belkhiri L, Bollinger J-C, Bouzaza A, Assadi A, Tirri A, Dahmoune F, Madani K, Reminie H. Removal of Methylene Blue from aqueous solutions by adsorption on Kaolin, Kinetic and equilibrium studies. Appl Clay Sci. 2018, 153, 38-45.
- [35] Hall KR, Eagleton LC, Acrivos A, Vermeulen T. Pore and soliddiffusion kinetics in fixed-bed adsorption under constant-pattern conditions. Ind Eng Chem Fundam. 1966, 5, 212-223.
- [36] Freundlich HM. Over the adsorption in solution. J Phys Chem A. 1906, 57, 385-470.
- [37] Temkin M J, Pyzhev V. Recent modifications to Langmuir isotherms. Acta physicochimica URSS. 1940, 12, 217-225.
- [38] Dubinin M M, Radushkevich LV. Equation of the characteristic curve of activated charcoal. Proceedings of the Academy of Sciences of the USSR. 1947, 55, 331-337.
- [39] Zhao H, Yan H, Zhang C, Liu X, Xue Y, Qiao Y, Tian Y, Qin S. Pyrolytic characteristics and kinetics of *Phragmites australis*. Evid Based Complement Alternat Med. 2011, 2011, 408973.
- [40] El Shahawy A, Heikal G. Organic pollutants removal from oily wastewater using clean technology economically, friendly biosorbent (*Phragmites australis*). Ecol Eng. 2018, 122, 207-218.
- [41] Melo DDQ, Neto VDOS, Barros FCDF, Raulino GSC, Vidal CB, do Nascimento RF. Chemical modifications of lignocellulosic materials and their application for removal of cations and anions from aqueous solutions. J Appl Polym Sci. 2016, 133(15).
- [42] Lu P, Hsieh YL. Multiwalled carbon nanotube (MWCNT) reinforced cellulose fibers by electrospinning. ACS Appl Mater Interfaces. 2010, 2(8), 2413-2420.
- [43] Kim D-Y, Lee B-M, Koo DH, Kang P-H, Jeun J-P. Preparation of nanocellulose from a kenaf core using E-beam irradiation and acid hydrolysis. Cellulose. 2016, 23(5), 3039-3049.
- [44] Barakat A, Mayer-Laigle C, Solhy A, Arancon RAD, de Vries H, Luque R. Mechanical pretreatments of lignocellulosic biomass, towards facile and environmentally sound technologies for biofuels production. RSC Adv. 2014, 4(89), 48109-48127.
- [45] Chen JP, Wu S, Chong K-H. Surface modification of a granular activated carbon by citric acid for enhancement of copper adsorption. Carbon. 2003, 41(10), 1979-1986.
- [46] Reddy KO, Guduri BR, Rajulu AV. Structural characterization and tensile properties of Borassusfruit fibers. J Appl Polym Sci. 2009, 114(1), 603-611.
- [47] Uma Maheswari C, Obi Reddy K, Muzenda E, Guduri BR, Varada Rajulu A. Extraction and characterization of cellulose microfibrils

- from agricultural residue *Cocos nucifera* L. Biomass and Bioenergy. 2012, 46, 555-563.
- [48] Pappas C, Tarantilis, PA, Daliani I, Mavromustakos T, Polissiou M. Comparison of classical and ultrasound-assisted isolation procedures of cellulose kenaf from (*Hibiscus cannabinus* L.) and eucalyptus (*Eucalyptus rodustrus* spp.). Ultrason Sonochem. 2002, 9(1), 19-23.
- [49] Alemdar A, Sain M. Isolation and characterization of nanofibers from agricultural residues, wheat straw and soy hulls. Bioresour Technol. 2008, 99(6), 1664-1671.
- [50] Hevira L, Zilfa, Rahmayeni, Ighalo JO, Aziz H, Zein R. *Terminalia catappa* shell as low-cost biosorbent for the removal of methylene blue from aqueous solutions. J Ind Eng Chem. 2021, 97, 188-199.
- [51] Reddy DHK., Harinath Y, Seshaiah K, Reddy AVR. Biosorption of Pb(II) from aqueous solutions using chemically modified *Moringa oleifera* tree leaves. Chem Eng Sci. 2010, 162, 626-634.
- [52] Nazir H, Salman M, Athar M, Farooq U, Wahab A, Akram M. Citric acid functionalized bougainvillea spectabilis, a novel, sustainable, and cost-effective biosorbent for removal of heavy metal (Pb<sup>2+</sup>) from waste water. Water Air Soil Pollut. 2019, 230, 303.
- [53] Lima EC, Royer B, Vaghetti JC, Simon NM, da Cunha BM, Pavan FA, et al. Application of Brazilian pine-fruit shell as a biosorbent to removal of reactive red 194 textile dye from aqueous solution kinetics and equilibrium study. J Hazard Mater. 2008, 155(3), 536-550.
- [54] Hameed BH, Ahmad AA. Batch adsorption of methylene blue from aqueous solution by garlic peel, an agricultural waste biomass. J Hazard Mater. 2009, 164(2-3), 870-875.
- [55] Abd El- Latif MM, Ibrahim AM. Adsorption, kinetic and equilibrium studies on removal of basic dye from aqueous solutions using hydrolyzed Oak sawdust. Desalin Water Treat. 2012, 6(1-3), 252-268.
- [56] Pathania D, Sharma S, Singh P. Removal of methylene blue by adsorption onto activated carbon developed from *Ficus carica* bast. Arab J Chem. 2017, 10, S1445-S1451.
- [57] Vilar V, Botelho C, Boaventura R. Methylene blue adsorption by algal biomass based materials, biosorbents characterization and process behaviour. J Hazard Mater. 2007, 147(1-2), 120-132.
- [58] Kankılıç GB, Metin AÜ, Tüzün İ. *Phragmites australis*, an alternative biosorbent for basic dye removal. Ecol Eng. 2016, 86, 85-94.
- [59] Al-Ghouti M, Khraisheh MA, Ahmad MN, Allen S. Thermodynamic behaviour and the effect of temperature on the removal of dyes from aqueous solution using modified diatomite, a kinetic study. J Colloid Interface Sci. 2005, 287(1), 6-13.
- [60] Maneerung T, Liew J, Dai Y, Kawi S, Chong C, Wang CH. Activated carbon derived from carbon residue from biomass gasification and its application for dye adsorption, Kinetics, isotherms and thermodynamic studies. Bioresour Technol. 2016, 200, 350-359.
- [61] Liu X, He C, Yu X, Bai Y, Ye L, Wang B, Zhang L. Net-like porous activated carbon materials from shrimp shell by solution-processed carbonization and H<sub>3</sub>PO<sub>4</sub> activation for methylene blue adsorption. Powder Technol. 2018, 326, 181-189.
- [62] Mattson J, Mark H. Activated carbon, surface chemistry and adsorption from carbon. Marcel Dekker, Ins., New York, 1971.
- [63] Gong J, Liu J, Jiang Z, Wen X, Mijowska E, Tang T, Chen X. A facile approach to prepare porous cup-stacked carbon nanotube with high performance in adsorption of methylene blue. J Colloid Interface Sci. 2015, 445, 195-204.
- [64] Danish M, Ahmad T, Majeed S, Ahmad M, Ziyang L, Pin Z, Shakeel Iqubal SM. Use of banana trunk waste as activated carbon in scavenging methylene blue dye, kinetic, thermodynamic, and isotherm studies. Bioresour Technol Rep. 2018, 3, 127-137.